PHYSICAL SCIENCES

Topologically protected optical polarization singularities in four-dimensional space

Christina M. Spaegele[1]*, Michele Tamagnone[1,2]*, Soon Wei Daniel Lim[1], Marcus Ossiander[1], Maryna L. Meretska[1], Federico Capasso[1]*

Optical singularities play a major role in modern optics and are frequently deployed in structured light, super-resolution microscopy, and holography. While phase singularities are uniquely defined as locations of undefined phase, polarization singularities studied thus far are either partial, i.e., bright points of well-defined polarization, or are unstable for small field perturbations. We demonstrate a complete, topologically protected polarization singularity; it is located in the four-dimensional space spanned by the three spatial dimensions and the wavelength and is created in the focus of a cascaded metasurface-lens system. The field Jacobian plays a key role in the design of such higher-dimensional singularities, which can be extended to multidimensional wave phenomena, and pave the way for unconventional applications in topological photonics and precision sensing.

INTRODUCTION

The field of singular optics explores the wide range of physics linked to phase and polarization singularities in electromagnetic fields (*1–7*) and has led to a wide range of applications (*8–11*). The definition of phase singularities is unambiguous: It describes points of vanishing amplitude and undefined phase in a complex scalar field (*2, 12, 13*). Examples of phase singularities include Laguerre-Gaussian beams (with azimuthal index $m \neq 0$), which carry orbital angular momentum (OAM) and have lines of zero intensity and undefined phase along their optical axes (*4*).

Polarization singularities in monochromatic fields, on the other hand, have a multivalent definition in the literature, requiring only one or more parameters of the polarization ellipse (e.g., azimuthal angle and ellipticity angle) to be singular (*1, 4, 8, 14–22*). They cannot be considered as complete polarization singularities as the polarization is either still defined at the singularity {e.g., L lines and bright C points [(*22*) and the Supplementary Materials]} or singular only in a specific basis and not topologically protected {e.g., V points, dark C points [(*8*) and the Supplementary Materials]}. They are, hence, easily destroyed by perturbations arising from many sources, such as stray light and device defects, which have the effect of adding or subtracting complex fields. Such fragility greatly limits their useful application range.

The shortcomings of the polarization singularities investigated so far call for research into the existence and design of complete polarization singularities, i.e., topologically protected points where the polarization is not defined. Polarization patterns have been explored in two-dimensional (2D) and 3D configurations (the latter including the phase degree of freedom) in Poincaré beams, skyrmions, and unstable singular membranes (*23–25*), as well as in the closely related field of topological photonics (*26–28*). Our aim here is instead to create a fully topologically protected, complete polarization singularity in structured light fields.

Conversely, one can already find topologically protected phase singularities in random complex scalar fields such as the speckle patterns of polarized monochromatic light reflected by a nonpolarizing random medium (*13, 29–31*). If the speckle pattern is projected onto a 2D screen, several points of vanishing amplitude and undefined phase appear. Sufficiently small perturbations in the field (e.g., by the addition of stray plane waves) do not destroy these phase singularities but only displace them in space. The stability of these singularities against small field perturbations is guaranteed by the topological structure of wave fields; we call these singular structures topologically protected and they are associated with quantized invariant values known as the topological charge. The only way to eliminate such singularities is to use a perturbation that is strong enough to bring together topological charges of opposite sign. This overlap will cause these singular structures to annihilate (*13, 32*).

In this work, we begin with a close elucidation of the protection mechanism for speckle patterns in the 2D transverse plane spanned by two Cartesian dimensions. We demonstrate that complete polarization singularities are not protected against perturbations in 2D and even 3D physical spaces. A higher-dimensional space is required to achieve such protection. It has been shown that any physical property of light (such as wavelength or angular momentum) or system parameter can be used as a synthetic dimension to extend the 3D Cartesian space, which creates many opportunities for rich and profound topological photonics effects (*33*). Using such a 4D synthetic space formed by the three spatial dimensions and the wavelength of light, we show that a topologically protected complete polarization and phase singularity can be achieved by a direct generalization of the phase singularity protection concept in two dimensions. These complete polarization singularities have a well-defined higher-dimensional topological charge.

We have realized complete polarization singularities using subwavelength-spaced arrays of optical elements (metasurfaces) and probed their topological protection with respect to stray light and device imperfections. The metasurface is designed to create an ellipsoid of light in the focal region of an aspheric lens with a complete and topologically protected polarization singularity at its center.

[1]Harvard John A. Paulson School of Engineering and Applied Sciences, Harvard University, Cambridge, MA, USA. [2]Fondazione Istituto Italiano di Tecnologia, Genova, Italy.
*Corresponding author. Email: capasso@seas.harvard.edu (F.C.); michele.tamagnone@iit.it (M.T.); spaegele@seas.harvard.edu (C.M.S.)

Spatially resolved measurements of the polarization in the focal region demonstrate the existence of all possible polarization states around the singularity. We perturb the field at and around the singularity by adding a perturbative polarized field at the singularity position. The singularity is experimentally observed to be topologically protected against such perturbations. Last, we discuss the applications of this generalized class of optical fields to stimulated emission depletion (STED) microscopy, optical metrology, and advancing the fundamental understanding of optical field topology.

RESULTS

Generalizing phase singularities

We will build up to the complete polarization singularity geometry in 4D space by first examining the migration of the zeros of a simple 1D function when it is perturbed. Then, we will extend these observations to the 2D phase singularity. Last, we will generalize the findings to design and characterize the polarization singularity in 4D space. For all these descriptions, we will only consider the class of twice continuously differentiable fields (C^2), which is justified as we can write steady-state electromagnetic waves in free space as the linear superposition of a finite number of plane waves. Here, regular type indicates scalars, boldface type indicates vectors (e.g., $\boldsymbol{E}$), and overlines (e.g., $\bar{\bar{J}}$) indicate matrices and tensors.

We begin with an arbitrary 1D real-valued function $f: \mathbb{R}^1 \mapsto \mathbb{R}^1$ (Fig. 1A). One can classify the zeros of f [i.e., $f(x_0) = 0$] into three categories, assigning them a simple topological charge m_{1D} that is dependent on the function's sign changes when crossing the zero: $m_{1D} = 1$ if the function changes from negative to positive, $m_{1D} = -1$ if it changes from positive to negative, and $m_{1D} = 0$ if the function is tangent to the axis at the zero but does not cross it. This topological charge can be formalized as

$$m_{1D} = \lim_{\mu \to 0} \frac{\text{sign}[f(x_0 + \mu)] - \text{sign}[f(x_0 - \mu)]}{2} \qquad (1)$$

As necessary for topological invariants, m_{1D} can be summed across a domain $[x_1, x_2]$ to yield information about the domain itself (34). This sum is conserved under continuous deformations (i.e., smooth transformation of the domain boundaries), as long as the domain boundaries do not coincide with the zero points.

Suppose an infinitesimal, uniform, real-valued perturbation $\varepsilon > 0$ (with $\varepsilon \in \mathbb{R}^1$) is added to f (Fig. 1B). This perturbation cannot destroy a zero with $m_{1D} = \pm 1$ as one is guaranteed to find a nearby field value that cancels the perturbing field and thus moves the zero to that new position. The only way to destroy a zero with $m_{1D} = \pm 1$ through a uniform perturbation is to increase the perturbation strength to merge and annihilate two zeros of opposite charge, as can be seen from Fig. 1A, by shifting the function upward or downward. In contrast, zeros with $m_{1D} = 0$ (for instance, second-order zero in Fig. 1B) are not protected against perturbations: They either immediately annihilate or split into two zero points of opposite charge ($m_{1D} = \pm 1$) (35). These $m_{1D} = 0$ zero points are, hence, infinitely rare under experimental conditions. A system can be designed to reach this edge case in theory, but in practice, it will not be perfectly realized because of experimental imperfections.

We also notice that near first-order zeros [i.e., $f'(x_0) \neq 0$], one can approximate the function linearly by $f(x) = f'(x_0) (x - x_0)$,

and the topological charge simplifies to $m_{1D} = \text{sign} [f'(x_0)]$ (36). That means that for first-order zeros, the first derivative value is sufficient to fully describe the topological properties of the zero. Uniform infinitesimal perturbations will not destroy the zero but offset it by an amount $\Delta x = -\varepsilon/f'(x_0)$. We will see that this is true also in higher dimensions. For higher-order zeros [$f'(x_0) = 0$], the protection depends on the detailed behavior of the higher derivatives. We summarize these observations by stating that a zero of the 1D real-valued function is topologically protected if its first derivative is nonvanishing at the point, and that this zero is associated with a topologically invariant quantity connected to the sign of the derivative.

The concepts of perturbation protection apply analogously to a 2D complex–valued function $\boldsymbol{E_x}: \mathbb{R}^2 \mapsto \mathbb{R}^2$ and can be used to describe phase singularities in speckle patterns on a 2D screen. Assuming monochromatic light and horizontal polarization, the complex scalar electric field E_x can be represented by its real ($\Re$) and imaginary ($\Im$) parts $\boldsymbol{E_x} = (E_{x\Re}, E_{x\Im})^T$, which depend on the position $\boldsymbol{u} = (x, y)^T$ on the screen (37). The speckle pattern shown in Fig. 1C is obtained by adding together sinusoids of different spatial frequencies, amplitudes, and phases. Singular positions occur where $|\boldsymbol{E_x}(\boldsymbol{u})| = 0$ with the phase $\phi = \arg(E_{x\Re} + iE_{x\Im}) = \text{atan } 2(E_{x\Im}, E_{x\Re})$ being undefined at these positions. The phase of the field changes azimuthally around these singularities, which are associated with a positive or negative topological charge depending on their orientation (2). In 2D, the total topological charge inside a region bounded by a curve C is typically determined as the phase accumulation along C (i.e., $m_{2D} = \frac{1}{2\pi} \oint_C \nabla\phi \cdot d\boldsymbol{l}$), where C by convention is taken counterclockwise (e.g., green curve in Fig. 1C). This is equivalent to the winding number [(3, 4), detailed description in the Supplementary Materials]. The topological charge of a singularity is defined by taking an infinitesimally small curve C around it.

In analogy to the 1D case, we can write the Taylor expansion around a singularity located at $\boldsymbol{u_0}$ as $\boldsymbol{E_x}(\boldsymbol{u}) = \bar{\bar{J}}(\boldsymbol{u} - \boldsymbol{u_0})$, replacing the derivative by the Jacobian matrix $\bar{\bar{J}}$, defined as

$$\bar{\bar{J}} = \begin{pmatrix} \dfrac{\partial E_{x\Re}}{\partial x} & \dfrac{\partial E_{x\Re}}{\partial y} \\ \dfrac{\partial E_{x\Im}}{\partial x} & \dfrac{\partial E_{x\Im}}{\partial y} \end{pmatrix} \qquad (2)$$

and considering its determinant. Note that this definition is consistent with the traditional definition of $m = \pm 1$ OAM line phase singularities: Close to the singularity, the complex scalar field is approximately $E_x(r, \theta) = re^{\pm i\theta} = r(\cos\theta \pm i\sin\theta) \approx x \pm iy$, up to an overall scale factor. In this case, the Jacobian is

$$\bar{\bar{J}} = \begin{pmatrix} 1 & 0 \\ 0 & \pm 1 \end{pmatrix} \qquad (3)$$

and the determinant equals ± 1.

In direct analogy to the 1D case, there are two cases: For first-order zeros, i.e., $\det(\bar{\bar{J}}) \neq 0$, the Jacobian is sufficient to fully describe the topological properties of the zero, and the topological invariant becomes $m_{2D} = \text{sign} [\det(\bar{\bar{J}})]$. For higher-order zeros, i.e., $\det(\bar{\bar{J}}) = 0$, the topological charge can be determined only by examining the higher-order derivatives (13, 29). To better illustrate this for the simulated speckle pattern in Fig. 1C, we plot $\det(\bar{\bar{J}})$ in Fig. 1D and notice that zeros with positive topological charges are always in a region of positive $\det(\bar{\bar{J}})$, and vice versa.

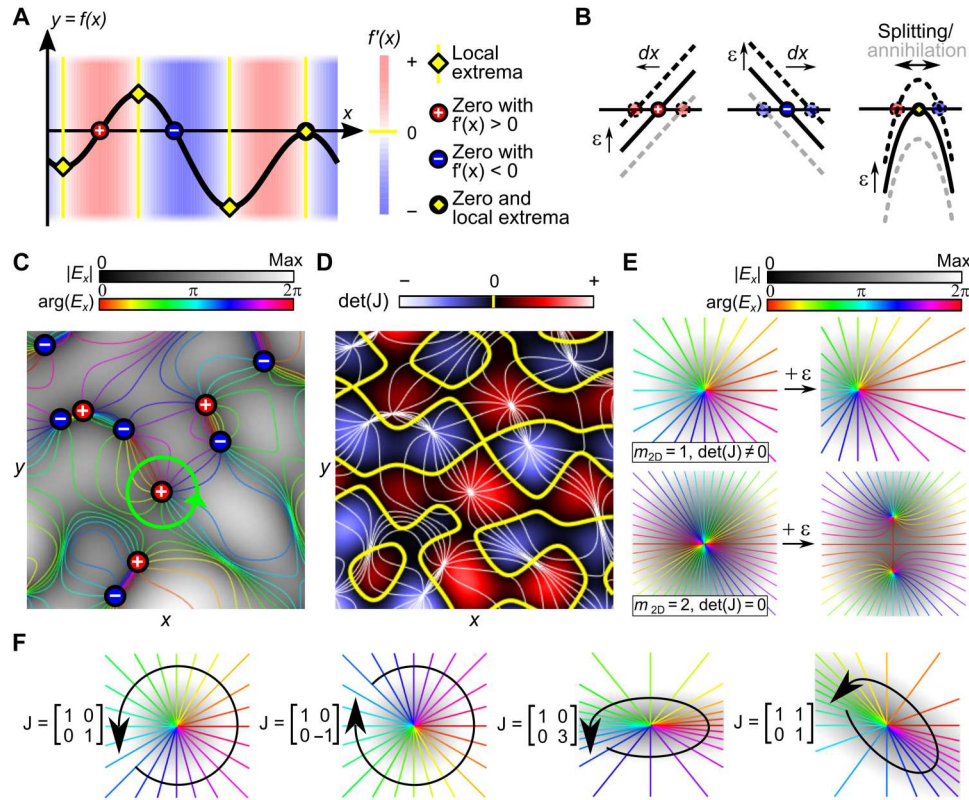**Fig. 1. Generalization of phase singularities.** (**A**) A simple 1D function with marked zeros and local extrema. (**B**) Only zeros with a nonzero derivative (topological charge, $m_{1D} = \pm 1$) are robust with respect to an infinitesimal perturbation ε (left and middle). Zeros that coincide with an extremum ($m_{1D} = 0$, right) are not topologically protected and either disappear or are split into multiple zeros of opposite charge when the perturbation is added. (**C**) Simulation of a random speckle pattern projected on a screen, showing the field's amplitude and phase. Equiphase lines intersect at singularities, i.e., points of vanishing amplitude and undefined phase. The phase increases azimuthally from 0 to 2π around the singularities with a clockwise (counterclockwise) increase in phase corresponding to a negative (positive) topological charge (highlighted respectively). Note that only zeros with a $\pm 2\pi$ phase accumulation around the singularity are found in speckle patterns, corresponding to $m_{2D} = \pm 1$. (**D**) The same speckle pattern as in (C), plotting the Jacobian determinant (see the main text); each positive singularity falls in a region of positive determinant ($m_{2D} = 1$) and vice versa. (**E**) While singularities with $m_{2D} = \pm 1$ are topologically protected against an additive infinitesimal perturbation ε to the field, singularities with $m_{2D} = 0$ are destroyed or break into multiple singularities of opposite charges. They are hence not observed in random fields and do not appear in the speckle pattern shown in (C). (**F**) The field around the singularity can be described by the Jacobian and does not need to be circularly symmetric.

In analogy to 1D zeros, singularities of this 2D complex field with $m_{2D} = \pm 1$ are topologically protected because they are surrounded by field values of all complex phases (Fig. 1E, top). This means that for an arbitrary small perturbing field dE, we can find a nearby point $\boldsymbol{u}'$ in the plane where the field value is $E(\boldsymbol{u}') = -dE$ to cancel out this perturbing field so that $\boldsymbol{u}'$ is the new singularity location after the perturbation. Higher-order singularities, on the other hand, are not topologically protected and are either destroyed or split into multiple simple singularities with $m_{2D} = \pm 1$ by the perturbation (Fig. 1E, bottom).

The Jacobian plays a critical role in understanding and justifying topological protection of first-order zeros. Starting with the Taylor expansion in the vicinity of the singularity, $\boldsymbol{E_x} = \bar{\bar{J}}(\boldsymbol{u} - \boldsymbol{u_0})$, an additive small perturbation $\boldsymbol{\varepsilon}$ changes the field to

$$\boldsymbol{E'_x} = \bar{\bar{J}}(\boldsymbol{u} - \boldsymbol{u_0}) + \varepsilon = \bar{\bar{J}}(\boldsymbol{u} - \boldsymbol{u_0} + \bar{\bar{J}}^{-1}\varepsilon) = \bar{\bar{J}}(\boldsymbol{u} - \boldsymbol{u_0}') \quad (4)$$

For a well-defined, unique $\bar{\bar{J}}^{-1}$, the singularity is hence moved by an amount $\bar{\bar{J}}^{-1}\varepsilon$ and is now positioned at $\boldsymbol{u'_0} = \boldsymbol{u_0} - \bar{\bar{J}}^{-1}\varepsilon$. Therefore, a singularity is maximally protected (i.e., the singularity position changes the least upon perturbation) if it is surrounded by a large region of a uniform, uniquely invertible Jacobian with large determinant as $\left[\bar{\bar{J}}^{-1} \sim \frac{1}{\det(\bar{\bar{J}})}\right]$. Note that $\bar{\bar{J}}^{-1}$ is unique and well defined only if $\bar{\bar{J}}$ is a square matrix and if $\det(\bar{\bar{J}})$ is not zero. A well-defined, unique $\bar{\bar{J}}^{-1}$ further ensures that all phases are found around the singularity. A small, arbitrary field $dE_x = a(\cos\theta, \sin\theta)^T$ with amplitude a and phase θ is located at the unique offset $d\boldsymbol{u} = -\bar{\bar{J}}^{-1}dE_x$ from the singularity.

Figure 1F shows that the field around the phase singularity changes with the Jacobian and does not need to be circularly symmetric. The orientation, ellipticity, and rotation of the field are determined by the singular value decomposition (SVD) of the Jacobian (Supplementary Materials).

We summarize the connection between topological protection and the nonvanishing of the Jacobian by stating that the topological protection of a singular point of $\boldsymbol{E_x}: \mathbb{R}^2 \mapsto \mathbb{R}^2$ can be ensured if the determinant of the Jacobian is nonvanishing at the point (full proofs in the Supplementary Materials). While it has been described before

that the sign of the Jacobian can define the topological charge for charge-one singularities (*13*, *29*), in this work, we are focusing on the role of the Jacobian to control the protection behavior and extend the concept of protection to higher dimensions.

These conclusions apply more generally whenever zeros are considered for $f: \mathbb{R}^N \to \mathbb{R}^N$, as the corresponding Jacobian is a square matrix that allows a unique inverse if the determinant is nonzero. While the topological invariant in the 1D case was concerned with the function behavior at points to the left and right of the singularity (more precisely, at the boundary of a 1D interval), and that of the 2D case was based on the function's behavior on a closed contour (at the boundary of a 2D surface), the corresponding topological invariants for the N-dimensional case now correspond to function behavior at the boundary of an N-dimensional volume containing the singularity. In the parlance of algebraic topology, this invariant is known as the topological degree (*38*) of the function boundary, which is equal to the sum of the topological charges of the singularities inside the volume. For first-order singularities, the sign of the determinant is the topological charge. These higher-dimensional invariants are described further in the Supplementary Materials.

We can now use the acquired knowledge about the protection mechanism in two dimensions to design a topologically protected polarization singularity. If we consider polarized light beams propagating along a direction z within the paraxial approximation (i.e., the z component of the field is negligible), the electric field vector consists of four real components at each point in space, namely, the real and imaginary parts of the x and y components of the field: $\boldsymbol{E} = (E_{x\Re}, E_{x\Im}, E_{y\Re}, E_{y\Im})^T$. All four components must be zero at the polarization singularity. In the nonparaxial domain, this condition would still allow the field's z component to be nonzero, which would correspond to an L line in 3D Cartesian space (*39*) and an L surface in 4D (Supplementary Materials). However, since every system can approach the paraxial limit with an additional lens included (Supplementary Materials), we design the experiment to be firmly in the paraxial regime, justifying the assumption of $|E_z| = 0$. Since the Jacobian $\overline{\overline{J}}$ that can be used to describe the field $\boldsymbol{E}(\boldsymbol{u}) = \overline{\overline{J}}(\boldsymbol{u} - \boldsymbol{u_0})$ can only be uniquely invertible if $\overline{\overline{J}}$ is a square matrix, we must match the number of "dimensions" to the number of constraints on the complex field components. As $\boldsymbol{E}$ is 4D, it is hence necessary to consider a 4D space $\boldsymbol{u}$, which replaces the 2D screen in the case of the speckle patterns. This can be realized by the three usual spatial dimensions plus the wavelength of light: $\boldsymbol{u} = (x, y, z, \lambda)^T$.

The wavelength dependence intended here assumes that the system is illuminated by a light source with tunable wavelength. As a direct extension of the 2D case, topological charges can again be defined as the degree of the function $\boldsymbol{E}(\boldsymbol{u}) = (E_{x\Re}, E_{x\Im}, E_{y\Re}, E_{y\Im})^T$, which is again equivalent to the sign of the function's determinant for first-order singularity. A singularity in such a field $\boldsymbol{E}: \mathbb{R}^4 \to \mathbb{R}^4$ from (x, y, z, λ) to $E_{x\Re}, E_{x\Im}, E_{y\Re}, E_{y\Im}$) will be a polarization singularity since both transverse polarizations are undefined ($E_{x\Re} = E_{x\Im} = E_{y\Re} = E_{y\Im} = 0$). We can further engineer the 4×4 Jacobian to have a nonzero determinant (and hence a well-defined $\overline{\overline{J}}^{-1}$) to create topologically protected complete singularities that are robust against the addition of arbitrary polarized perturbations. A well-defined $\overline{\overline{J}}^{-1}$ further ensures that all transverse field phases and polarizations exist in the vicinity

of this singularity. Analogously to the lower-dimensional cases, we can locate a small, arbitrary field $d\boldsymbol{E} \in \mathbb{R}^4$ (and hence any combination of phase and polarization) at an offset $d\boldsymbol{u} = -\overline{\overline{J}}^{-1} d\boldsymbol{E}$ from the singularity position. Hence, the field evaluated at a given distance from the singularity consists of all polarizations and phases, as in skyrmionic hopfions (*23*). In the remainder of this paper, we will show how this type of singularity can be created and experimentally realized using metasurfaces.

Design of complete polarization singularities in 4D space

We chose to design the polarization singularity at the center of a focused light beam (Fig. 2A). The light field is generated by a polarization-sensitive metasurface illuminated with horizontally polarized light [(*40*) and the Supplementary Materials] and a cascaded aspheric convex lens. The polarization-sensitive metasurface behaves like a spatially varying waveplate and thus gives us control over the local polarization state in the near field of the metasurface with high spatial resolution (*41*). The convex lens relaxes design constraints on the metasurface since the metasurface is then not required to imprint a focusing phase profile. Our objective is a field distribution around the singularity that can be described by an invertible Jacobian matrix (i.e., $\det\overline{\overline{J}} \neq 0$) to ensure topological protection against perturbations.

We split the design procedure into two steps, starting with the spatial dimensions and later dealing with the wavelength dependence. As long as $\det\overline{\overline{J}} \neq 0$, the Jacobian and its constituent matrix elements can be chosen freely (including off-diagonal elements) without destroying the protection of the singularity. While strength and orientation of the field confinement can be designed using the SVD of the Jacobian (Supplementary Materials), for simplicity, we initially search for a design where the Jacobian is diagonal in the spatial elements. Let $(dx, dy, dz, d\lambda)^T$ be a displacement from the singularity position in 4D space. First, we consider the spatial structure of the singularity at the design wavelength $d\lambda = 0$. We can describe the field around the singularity as

$$
d\boldsymbol{E} = \begin{pmatrix} dE_{x\Re} \\ dE_{x\Im} \\ dE_{y\Re} \\ dE_{y\Im} \end{pmatrix} = \overline{\overline{J}} \begin{pmatrix} dx \\ dy \\ dz \\ d\lambda \end{pmatrix} = J_0 \begin{pmatrix} 1 & 0 & 0 & J_{14} \\ 0 & 1 & 0 & J_{24} \\ 0 & 0 & 1 & J_{34} \\ 0 & 0 & 0 & J_{44} \end{pmatrix} \begin{pmatrix} dx \\ dy \\ dz \\ 0 \end{pmatrix}
$$
$$
= J_0 \begin{pmatrix} dx \\ dy \\ dz \\ 0 \end{pmatrix} \tag{5}
$$

where J_0 is a constant with the dimensions of a field gradient.

Using spherical coordinates around the position of the singularity

$$
\begin{aligned}
dx &= dr\, \sin\theta\, \cos\phi \\
dy &= dr\, \sin\theta\, \sin\phi \\
dz &= dr\, \cos\theta
\end{aligned} \tag{6}
$$

this vector $d\boldsymbol{E}$ can also be represented by a complex Jones vector $|d\psi\rangle \in \mathbb{C}^2$ in the horizontal/vertical polarization basis
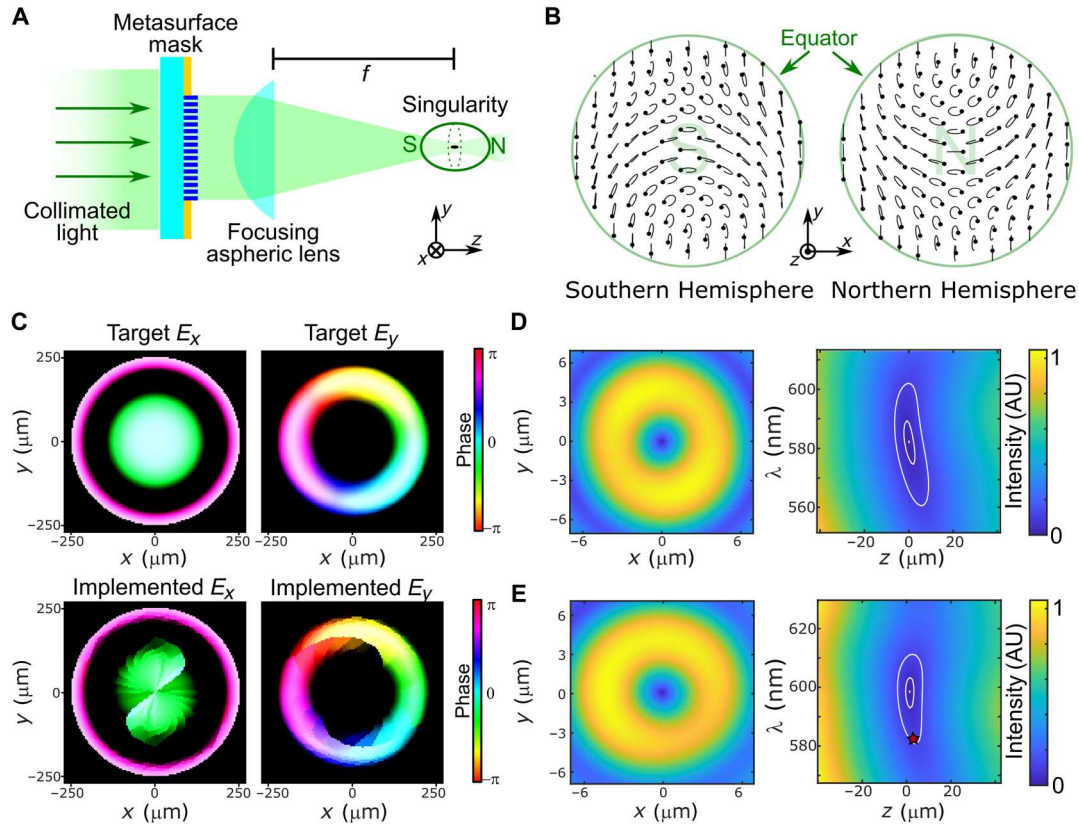
Fig. 2. Design of complete polarization singularities in 4D space. (**A**) A metasurface implements the required phase and polarization pattern, which is subsequently focused with an aspheric lens forming the singularity at its focus. The constant light amplitude contour of a cross section is shown encircling the singularity. (**B**) The polarization and phase (represented by a dot on the polarization ellipse) of the target electric field around the singularity. All polarizations exist twice on the ellipsoid, with pairs of identical polarization and intensity but opposite phase. This produces destructive interference at the singularity position. (**C**) Target and simulated electric field components at a distance of 1 μm from the metasurface (field's phase and intensity are represented by color and brightness, respectively). For each point in the target field, one can find exactly one other point of equal polarization, but with opposite phase, ensuring destructive interference at the asphere focus. (**D**) Simulated normalized intensity of the electric field in the xy and $z\lambda$ planes, showing a singularity of null field and its confinement (i.e., of surrounding increasing intensity) in all four dimensions. The contour lines join points of equal field strength. (**E**) Simulated normalized intensity of the electric field in the xy and $z\lambda$ planes when a field perturbation ε is added, which can arise from many sources, such as stray light and device defects. The singularity is shifted in the 4D space, but the singularity intensity minimum value remains the same. The red star marks the position of the unperturbed singularity in the $z\lambda$ plane. AU, arbitrary units.

(Supplementary Materials)

$$|d\psi\rangle = \begin{pmatrix} dE_{x\Re} + idE_{x\Im} \\ dE_{y\Re} + idE_{y\Im} \end{pmatrix} = J_0[(dx + idy)|\boldsymbol{H}\rangle + dz\,|\boldsymbol{V}\rangle]$$
$$= J_0 dr \begin{pmatrix} \sin\theta e^{i\phi} \\ \cos\theta \end{pmatrix} \qquad (7)$$

where $|\boldsymbol{H}\rangle = (1,0)^T$ and $|\boldsymbol{V}\rangle = (0,1)^T$ correspond to the horizontal and vertical basis vectors, respectively, and θ and φ range from 0 to π and 0 to 2π, respectively. The singularity described by Eq. 7 is surrounded by all possible polarization states at least twice on the sphere (more precisely the ellipsoid) around it (Fig. 2B), with point pairs positioned radially symmetric with respect to the singularity having the same polarization but opposite sign, i.e., representing transverse fields phase-shifted by π.

The required phase and polarization profile is mapped on the metasurface following an approach similar to the method used in super-resolution STED (*42*): In the absence of the metasurface, the impinging collimated light would constructively interfere at the focal position of the lens. The metasurface acts as a spatially varying waveplate that converts the impinging linearly polarized light into all polarizations on the Poincaré sphere (Fig. 2C). Immediately after the metasurface, there are pairs of radially symmetric points of equal polarization but opposite sign leading to destructive interference at the focus of the lens since the two polarization states have the same optical path length to the focus. When one moves away from the focal position, this optical path difference becomes nonzero for certain polarization pairs, leading to incomplete cancellation around the singularity resulting in the intensity and polarization distribution shown in Fig. 2B (see the Supplementary Materials for more details).

The metasurface is implemented by dividing the required profile into square unit cells of periodicity p = 420 nm. At each position, we choose the dimension and rotation of a meta-atom that most closely transforms the impinging linear polarized light to the required polarization and phase (i.e., matches the required Jones matrix most closely) at the design wavelength of λ_0 = 600 nm [(*40, 41, 43, 44*) and the Supplementary Materials]. We use a meta-atom library

consisting of 49,613 titanium dioxide nanofins of height $h = 600$ nm fabricated on a fused silica substrate.

Up to now, we have ensured that the singularity is surrounded by light (i.e., confined) in the 3D space, but we have not yet considered the last dimension λ. To ensure confinement in λ, we tune the chromatic dispersion of the metasurface by adding a constant global phase offset to the required Jones matrix profile. This global phase offset can be chosen freely as only phase differences between the meta-atoms matter. Changing the global phase over the whole metasurface Jones matrix profile hence does not change the polarization distribution implemented by the metasurface. Instead, the global phase changes the set of nanopillars chosen to implement the required profile. As the size of the library is finite, each set has a different combination of nanostructures, resulting in a different dispersion behavior as different nanofins have a different chromatic dispersion (Supplementary Materials). This allows us to maximize the singularity confinement in the wavelength dimension. Specifically, a higher dispersion implies a higher derivative of the fields with respect to the wavelength, so that the aforementioned destructive interference among all polarizations does not occur anymore for wavelengths different from λ_0.

We emphasize the importance of the dispersion engineering possible with metasurfaces (45) as it not only ensures that the Jacobian is invertible but also enables control of the confinement in the wavelength space. While tuning the global phase is sufficient to create confinement in λ, dispersion engineering methods described in (45) can further shape the confinement in λ. Implementing the Jones matrix profile selection without this dispersion design may lead to a zero (or very small) determinant of the Jacobian. In that case, a small perturbation could either destroy the singularity [if $\det(\bar{\bar{J}}) = 0$] or move the singularity to a displaced wavelength not reachable by our experimental setup.

Figure 2C shows the target and simulated electric field just after the metasurface. The implemented electric field is slightly different from the desired field due to the limited size of the meta-atom library. Simulations of the focal spot profile near the singularity (Fig. 2D), which include the focusing by an aspheric lens, confirm the existence of the complete polarization singularity in the 4D space (x, y, z, λ) (see the Supplementary Materials).

At the design wavelength, the singularity appears as a single point in the three spatial dimensions having null electric field, with all polarizations appearing twice in its immediate vicinity (see Fig. 2B) (Supplementary Materials). As mentioned above, the invertible Jacobian ensures that all polarization and phases are located in its immediate vicinity in 4D space and ensures its topological protection. The topological charge of the singularity is $m_{4D} = \text{sign}[\det(\bar{\bar{J}})] = -1$ (Supplementary Materials).

The only way to destroy the singularity by a constant perturbation is to merge two singularities of opposite sign. For this, one must push the singularity out of its surrounding region of increasing intensity, which acts like a shield protecting the singularity from destruction. Hence, the singularity is protected if the perturbation intensity is smaller than the intensity at the weakest point of this protection shield (i.e., for $0 < I \lesssim I_{max}/2$, with I_{max} being the maximum intensity of the surrounding field). Figure 2E shows the field intensity distribution resulting from the inclusion of an exemplary perturbation of amplitude $\varepsilon = \frac{\sqrt{I_{max}}}{3}(1, 0, 0, 1)^T$. While the

singularity position is shifted in the 4D space, the minimum intensity value remains constant.

Experimental validation

The metasurface (Fig. 3B) of diameter $d = 500$ μm was fabricated using the same process as described in (46, 47) (Supplementary Materials) on a fused silica substrate. The metasurface is illuminated by a collimated supercontinuum laser filtered by a tunable band-pass filter (bandwidth, 5 nm) to select visible wavelengths between 485 and 700 nm. The quality of the measurement depends on the monochromaticity of the light source, with the intensity measured at the singularity position decreasing with the bandwidth of the laser. An aluminum aperture mask ensures that no light is transmitted outside of the metasurface area. The light is then focused with an aspheric lens of numerical aperture (NA) = 0.08 and imaged through a 75× microscope (Fig. 3A). The spatially varying Stokes polarization state over transverse planes is retrieved using rotating quarter–wave plate polarimetry (48). A precise alignment of the components with respect to the optical axis is essential to observe the singularity with high contrast and was achieved with manual and motorized nanopositioners. The full 4D space (x, y, z, λ) can be explored by imaging the singularity for different z positions and wavelengths λ. The field distribution results (Fig. 3, C to E) confirm the theory and numerical predictions, showing a confinement of the singularity along all four dimensions; the relative intensity contrast is ~24 dB with respect to the intensity maximum, and all polarizations can be found on a small ellipsoid around the singularity (see Fig. 3, F and G, and the Supplementary Materials).

Topological protection

The fact that the singularity is topologically protected with respect to offsets in the fields provides robustness against perturbation. This also explains why the singularity was easily found experimentally despite imperfections in the metasurface fabrication process and experimental alignment. These imperfections did not destroy the singularity but simply shifted it in space and wavelength. To further observe the topological protection behavior of our singularity, we inserted a small opaque circular gold mask to shadow part of the metasurface. Different areas of the metasurface convert the impinging horizontally polarized light into different polarizations (see Figs. 2C and 4, A and D), with each polarization having exactly one counterpart of opposite phase on the metasurface, ensuring destructive interference at the focal spot of the aspheric lens. The partial shadowing suppresses the destructive interference of specific polarization pairs at the focus position and hence corresponds to adding polarized fields with opposite phase and different magnitude at the position of the singularity. Using a gold disk with a 110-μm diameter, both simulation (Fig. 4, B and E) and experiment (Fig. 4, C and F) show that the singularity persists despite the perturbation while being displaced in the 4D space, i.e., moving to a slightly different position and a slightly different wavelength.

DISCUSSION

These topologically protected polarization singularities are the direct generalization of phase singularities and can find applications in light structuring, super-resolution STED microscopy, and polarimetry since they transform the polarization changes of light induced by perturbations into the geometrical displacements of a
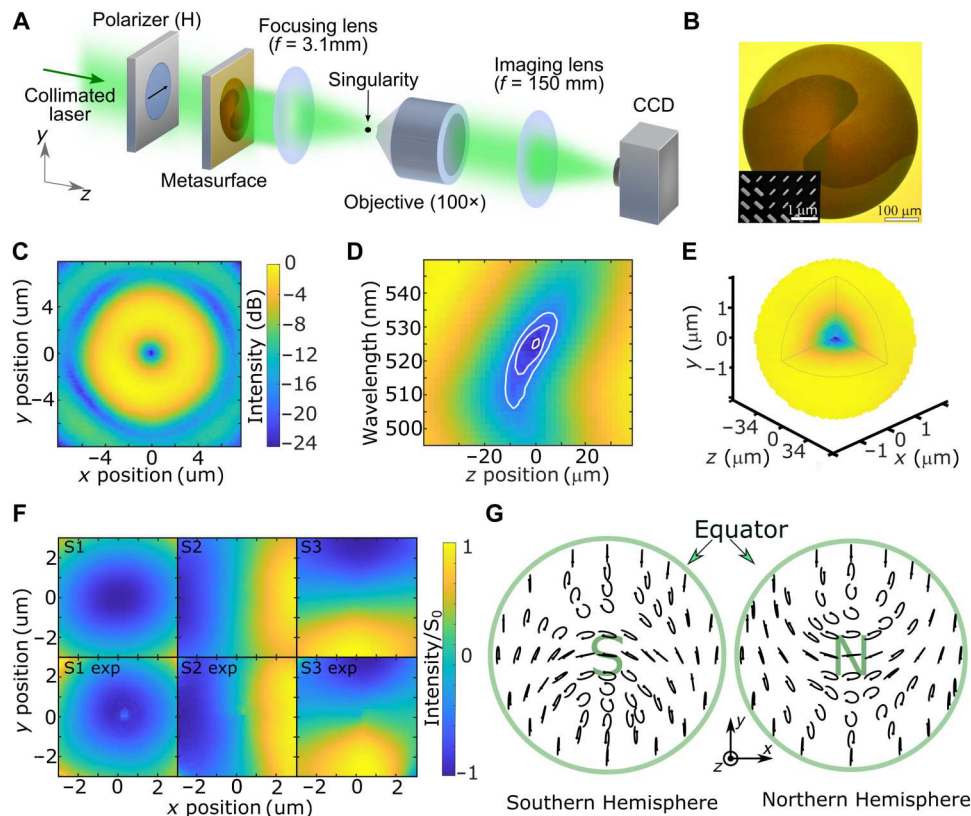
Fig. 3. Experiment. (**A**) The experimental setup. The singularity is generated as in Fig. 2A and then imaged with a microscope. A motorized stage is used to move the objective along the z direction. The light source is a supercontinuum laser with a tunable band-pass filter of 5-nm bandwidth used to explore different wavelengths. To retrieve the polarization distribution in the singularity region, a Stokes polarimeter consisting of rotating quarter–wave plate and a polarizer was placed between objective and imaging lens (fig. S15). (**B**) Microphotograph of the fabricated 500-μm-diameter metasurface surrounded by an aluminum mask. Inset, SEM image of a small metasurface region. (**C** to **E**) Intensity measurement showing a singularity that is confined in 4D space: (C) After determining the position (x_0, y_0, z_0, λ_0) of the singularity in the 4D space, an xy image was acquired at $\lambda_0 = 526$ nm, $z_0 = 0$ μm. The decibel (dB) scale is normalized with respect to the maximum intensity in the 4D dataset. Scale bar, 2 μm. (D) The same as (C) for the $z\lambda$ plane at $x_0 = 0$ μm, $y_0 = 0$ μm. (E) Sections of the 3D xyz space measured at $\lambda = \lambda_0$ showing that the singularity is fully surrounded by light. (**F**) Simulated (top) and measured (bottom) Stokes parameters normalized by its pixel-wise intensity S_0 at $z = z_0$, $\lambda = \lambda_0$. Scale bar, 1 μm, showing good agreement. (**G**) Polarization distribution measured on an ellipsoid of equal field intensity around the singularity (radius, 0.25 μm in the xy plane and length, 8 μm in the z direction, $\lambda = \lambda_0$), showing good agreement with the simulation (Fig. 2B).

tightly localized feature. The singularity could also have interesting applications in dark-field optical tweezer and in ion traps, where the position and trapping mechanism of the singularity can be actively tuned by displacing a gold disk perturbation in front of the metasurface or changing the impinging laser wavelength, respectively.

The tight localization of the dark spot at the center of the presented singularity means that the singularity spatial position can be measured with deeply subwavelength precision, better than that of bright regions of light (*49*). This behavior may pave the way for an expanded class of precision sensors that probe distant physical phenomena [such as position displacements (*50*)] by precisely monitoring minute beam perturbations in the vicinity of the singular region. The polarization and chromatic sensitivity of the complete polarization singularity expands the palette of detectable properties of light that can be deterministically correlated with the singularity position in the combined Cartesian/spectral domain.

More generally, our work paves the way for an expanded metasurface optics design paradigm based on engineering not only the light field amplitude but also its gradient to achieve fault-tolerant metasurface designs. Such architectures will be ideal for

environments with high damage probability, such as in plasma chambers (*51, 52*) and particle-laden media (*53*). Future work will investigate higher- and mixed-order singularities (i.e., singularities that have different topological charges depending on the considered spatial dimension). Last, our results are applicable to other design dimensions. For instance, the wavelength of light can be replaced by another free parameter of the system, such as the angle of incidence. The latter can be implemented using the same nomenclature introduced here with the substitution $\lambda \rightarrow k_{\parallel}$, where $k_{\parallel}$ is the tangential component of the impinging wave vector along the metasurface plane. We expect such a polarization singularity to have a similar protection strength due to the precise angular dispersion control capability of metasurfaces (*54*). The results are further applicable to other wave-like physical systems, as long as they can be represented as ($n + 1$)-times differentiable fields (C^{n+1}), where n is the order of the desired singularity.
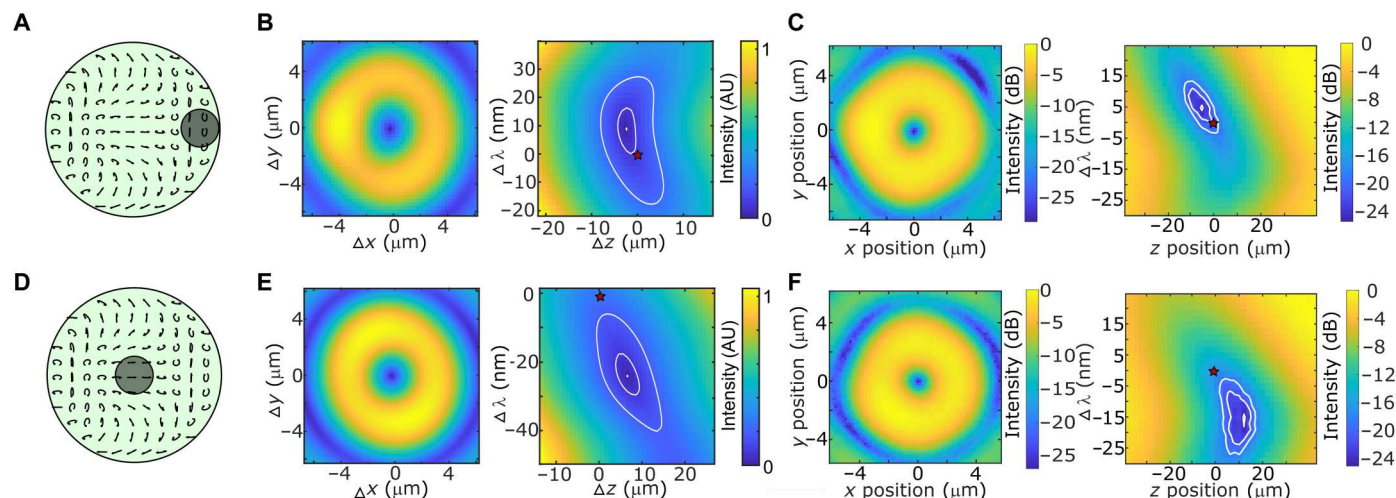
Fig. 4. Topological protection. (**A**) Schematic of the electric field polarization conversion implemented by the metasurface. Blocking part of the metasurface with a gold disk (position and size depicted with a light gray circle) corresponds to subtracting a perturbing polarized field, which can be used to probe the protection mechanism of the singularity. (**B**) Simulated normalized intensity of the electric field in the xy and $z\lambda$ planes after the perturbation is applied. The singularity is shifted in the $z\lambda$ plane, slightly distorting the field distribution around the singularity. As the field surrounding the singularity acts as a protection shield, the singularity moves closer to the edge of the shield when perturbed. The red star marks the position of the unperturbed singularity. The minimum intensity of the singularity remains the same upon perturbation. The origin of the coordinate system is the position of the simulated unperturbed singularity (red star marking the position of the unperturbed singularity in the $z\lambda$ plane). (**C**) Experimentally measured intensity of the electric field in the xy and $z\lambda$ plane resulting from the addition of the perturbation. The minimum intensity remains the same upon the addition of the perturbation, only shifting the singularity in position-wavelength space. The origin of the coordinate system is the position of the experimental unperturbed singularity (red star marking the position of the unperturbed singularity in the $z\lambda$ plane). Scale bar, 2 μm. (**D** to **F**) The same as (A) to (C), respectively, for a different gold disk position.

MATERIALS AND METHODS
Sample fabrication
To create the aluminum mask, we spin-coated LOR3A and S1805 photoresist on a 500-μm-thick SiO_2 substrate, exposed it using optical lithography everywhere except at the position of the metasurface, and subsequently developed it in MF319. After an oxygen plasma descum, we deposited 150 nm of aluminum and lifted it off by immersing it in Remover PG solution for 30 hours. Subsequently, we added another 50-nm-thick gold mask with a larger opening at its center following the same procedure for alignment-marker visibility during electron beam lithography. We then used our standard metasurface process (*46*, *47*) to create the metasurface pillars in the central opening of the mask (see the Supplementary Materials for a detailed process flow).

Numerical simulations
We created the metasurface pillar library using the rigorous coupled wave analysis solver Reticolo (*55*) and the refractive indices n_{SiO2} = 1.457 and n_{TiO2} = 2.346. The field calculations around the singularity were performed using MATLAB (see the Supplementary Materials for a detailed description of the simulations).

Measurements
The measurements were performed using a supercontinuum laser source. The source generates light in the visible region from 485 to 700 nm, which we filter using a tunable band-pass filter with 5 nm (full width at half maximum) bandwidth. We then focus the light with an aspheric lens (f = 3.1 mm, NA_{eff} = 0.08) and image the singularity using a 100× Nikon objective (NA = 0.9), an imaging lens (f = 15 cm), and a scientific CMOS camera (pixel size, 6.5 μm by 6.5 μm; dynamic range, 21,500:1).

Supplementary Materials
This PDF file includes:
Supplementary Text
Figs. S1 to S18
References

REFERENCES AND NOTES
1. G. J. Gbur, *Singular Optics* (CRC Press, 2016).
2. J. F. Nye, M. V. Berry, Dislocations in wave trains, in *A Half-Century of Physical Asymptotics and Other Diversions: Selected Works by Michael Berry* (World Scientific, 2017), pp. 6–31.
3. M. Soskin, S. V. Boriskina, Y. Chong, M. R. Dennis, A. Desyatnikov, Singular optics and topological photonics. *J. Opt.* **19**, 10401 (2016).
4. M. R. Dennis, K. O'holleran, M. J. Padgett, Singular optics: Optical vortices and polarization singularities, in *Progress in Optics* (Elsevier, 2009), vol. 53, pp. 293–363.
5. W. Whewell, Singular optics: More ado about nothing. *J. Opt. A: Pure Appl. Opt.* **11**, 090201 (2009).
6. A. S. Desyatnikov, Y. S. Kivshar, L. Torner, Chapter 5—Optical vortices and vortex solitons, in *Progress in Optics*, E. Wolf, Ed. (Elsevier, 2005), vol. 47, pp. 291–391.
7. M. V. Berry, Geometry of phase and polarization singularities illustrated by edge diffraction and the tides, in *Second International Conference on Singular Optics (Optical Vortices): Fundamentals and Applications* (Bellingham Washington, 2001), vol. 4403, pp. 1–12.
8. W. Liu, W. Liu, L. Shi, Y. Kivshar, Topological polarization singularities in metaphotonics. *Nanophotonics* **10**, 1469–1486 (2021).
9. Y. Shen, X. Wang, Z. Xie, C. Min, X. Fu, Q. Liu, M. Gong, X. Yuan, Optical vortices 30 years on: OAM manipulation from topological charge to multiple singularities. *Light Sci. Appl.* **8**, 90 (2019).
10. H. Rubinsztein-Dunlop, A. Forbes, M. V. Berry, M. R. Dennis, D. L. Andrews, M. Mansuripur, C. Denz, C. Alpmann, P. Banzer, T. Bauer, Roadmap on structured light. *J. Opt.* **19**, 13001 (2016).
11. A. H. Dorrah, F. Capasso, Tunable structured light with flat optics. *Science* **376**, eabi6860 (2022).
12. M. Vasnetsov, *Optical Vortices* (Nova Science Pub Incorporated, 1999), vol. 228.
13. M. V. Berry, M. R. Dennis, Phase singularities in isotropic random waves. *Proc. Math. Phys. Eng. Sci.* **456**, 2059–2079 (2000).

14. Q. Zhan, Cylindrical vector beams: From mathematical concepts to applications. *Adv. Opt. Photonics* **1**, 1–57 (2009).

15. J. F. Nye, Monstars on glaciers. *J. Glaciol.* **29**, 70–77 (1983).

16. J. F. Nye, *Natural Focusing and Fine Structure of Light: Caustics and Wave Dislocations* (CRC Press, 2000).

17. J. F. Nye, Lines of circular polarization in electromagnetic wave fields. *Proc. R. Soc. A Math. Phys. Sci.* **389**, 279–290 (1983).

18. J. F. Nye, J. V. Hajnal, The wave structure of monochromatic electromagnetic radiation. *Proc. R. Soc. A Math. Phys. Sci.* **409**, 21–36 (1987).

19. J. V. Hajnal, Singularities in the transverse fields of electromagnetic waves I. Theory. *Proc. R. Soc. A Math. Phys. Sci.* **414**, 433–446 (1987).

20. M. V. Berry, M. R. Dennis, Polarization singularities in isotropic random vector waves. *Proc. Math. Phys. Eng. Sci.* **457**, 141–155 (2001).

21. E. J. Galvez, Light beams with spatially variable polarization. *Photonics: Scientific Foundations, Technology and Applications* **1**, 61–76 (2015).

22. M. R. Dennis, Polarization singularities in paraxial vector fields: Morphology and statistics. *Opt. Commun.* **213**, 201–221 (2002).

23. D. Sugic, R. Droop, E. Otte, D. Ehrmanntraut, F. Nori, J. Ruostekoski, C. Denz, M. R. Dennis, Particle-like topologies in light. *Nat. Commun.* **12**, 6785 (2021).

24. S. W. D. Lim, J.-S. Park, M. L. Meretska, A. H. Dorrah, F. Capasso, Engineering phase and polarization singularity sheets. *Nat. Commun.* **12**, 4190 (2021).

25. A. J. Vernon, F. J. Rodriguez-Fortuño, Creating and moving nanoantenna cold spots anywhere. *Light Sci. Appl.* **11**, 1–10 (2022).

26. L. Lu, J. D. Joannopoulos, M. Soljačić, Topological photonics. *Nat. Photonics* **8**, 821–829 (2014).

27. B. Zhen, C. W. Hsu, L. Lu, A. D. Stone, M. Soljačić, Topological nature of optical bound states in the continuum. *Phys. Rev. Lett.* **113**, 257401 (2014).

28. M. Kim, Z. Jacob, J. Rho, Recent advances in 2D, 3D and higher-order topological photonics. *Light Sci. Appl.* **9**, 130 (2020).

29. M. R. Dennis, H. H. Wills, thesis, University of Bristol, Bristol, UK (2001).

30. J. Gâteau, F. Claude, G. Tessier, M. Guillon, Topological transformations of speckles. *Optica* **6**, 914–920 (2019).

31. K. O'holleran, M. R. Dennis, M. J. Padgett, Topology of light's darkness. *Phys. Rev. Lett.* **102**, 143902 (2009).

32. J. W. Goodman, *Speckle Phenomena in Optics: Theory and Applications* (Roberts and Company Publishers, 2007).

33. L. Yuan, Q. Lin, M. Xiao, S. Fan, Synthetic dimension in photonics. *Optica* **5**, 1396–1405 (2018).

34. A. F. Beardon, *Complex Analysis: The Argument Principle in Analysis and Topology* (Courier Dover Publications, 2019).

35. I. V. Basistiy, V. Y. Bazhenov, M. S. Soskin, M. V. Vasnetsov, Optics of light beams with screw dislocations. *Opt. Commun.* **103**, 422–428 (1993).

36. G. Fonseca, I. Fonseca, W. Gangbo, in *Degree Theory in Analysis and Applications* (Oxford Univ. Press, 1995), vol. 2.

37. M. Born, E. Wolf, *Principles of Optics: Electromagnetic Theory of Propagation, Interference and Diffraction of Light* (Elsevier, 2013).

38. A. S. Schwarz, *Topology for Physicists* (Springer Science & Business Media, 2013), vol. 308.

39. K. Tekce, E. Otte, C. Denz, Optical singularities and Möbius strip arrays in tailored nonparaxial light fields. *Opt. Express* **27**, 29685–29696 (2019).

40. J. P. B. Mueller, N. A. Rubin, R. C. Devlin, B. Groever, F. Capasso, Metasurface polarization optics: Independent phase control of arbitrary orthogonal states of polarization. *Phys. Rev. Lett.* **118**, 113901 (2017).

41. N. A. Rubin, Z. Shi, F. Capasso, Polarization in diffractive optics and metasurfaces. *Adv. Opt. Photonics* **13**, 836–970 (2021).

42. B. Harke, C. K. Ullal, J. Keller, S. W. Hell, Three-dimensional nanoscopy of colloidal crystals. *Nano Lett.* **8**, 1309–1313 (2008).

43. N. A. Rubin, G. D'Aversa, P. Chevalier, Z. Shi, W. T. Chen, F. Capasso, Matrix fourier optics enables a compact full-stokes polarization camera. *Science* **365**, eaax1839 (2019).

44. A. Zaidi, N. A. Rubin, A. H. Dorrah, J.-S. Park, F. Capasso, Generalized polarization transformations with metasurfaces. *Opt. Express* **29**, 39065–39078 (2021).

45. W. T. Chen, A. Y. Zhu, F. Capasso, Flat optics with dispersion-engineered metasurfaces. *Nat. Rev. Mater.* **5**, 604–620 (2020).

46. M. Khorasaninejad, W. T. Chen, R. C. Devlin, J. Oh, A. Y. Zhu, F. Capasso, Metalenses at visible wavelengths: Diffraction-limited focusing and subwavelength resolution imaging. *Science* **352**, 1190–1194 (2016).

47. R. C. Devlin, M. Khorasaninejad, W. T. Chen, J. Oh, F. Capasso, Broadband high-efficiency dielectric metasurfaces for the visible spectrum. *Proc. Natl. Acad. Sci. U.S.A.* **113**, 10473–10478 (2016).

48. B. Schaefer, E. Collett, R. Smyth, D. Barrett, B. Fraher, Measuring the Stokes polarization parameters. *Am. J. Phys.* **75**, 163–168 (2007).

49. H. Wolter, Concerning the path of light upon total reflection. *J. Opt. A Pure Appl. Opt.* **11**, 090401 (2009).

50. G. H. Yuan, N. I. Zheludev, Detecting nanometric displacements with optical ruler metrology. *Science* **364**, 771–775 (2019).

51. E. Langereis, S. B. S. Heil, M. C. M. van de Sanden, W. M. M. Kessels, In situ spectroscopic ellipsometry study on the growth of ultrathin TiN films by plasma-assisted atomic layer deposition. *J. Appl. Phys.* **100**, 023534 (2006).

52. J. Linke, J. Du, T. Loewenhoff, G. Pintsuk, B. Spilker, I. Steudel, M. Wirtz, Challenges for plasma-facing components in nuclear fusion. *Matter Radiat. Extremes* **4**, 056201 (2019).

53. U. V. Nägerl, T. Bonhoeffer, Imaging living synapses at the nanoscale by STED microscopy. *J. Neurosci.* **30**, 9341–9346 (2010).

54. Z. Shi, A. Y. Zhu, Z. Li, Y.-W. Huang, W. T. Chen, C.-W. Qiu, F. Capasso, Continuous angle-tunable birefringence with freeform metasurfaces for arbitrary polarization conversion. *Sci. Adv.* **6**, eaba3367 (2020).

55. J. P. Hugonin, P. Lalanne, Reticolo software for grating analysis, preprint arXiv:2101.00901 (2021).

56. P. Senthilkumaran, S. K. Pal, Phase singularities to polarization singularities. *Int. J. Opt.* **2020**, 1–33 (2020).

57. S. W. Hell, J. Wichmann, Breaking the diffraction resolution limit by stimulated emission: Stimulated-emission-depletion fluorescence microscopy. *Opt. Lett.* **19**, 780–782 (1994).

Science Advances

Topologically protected optical polarization singularities in four-dimensional space

Christina M. Spaegele, Michele Tamagnone, Soon Wei Daniel Lim, Marcus Ossiander, Maryna L. Meretska, and Federico Capasso

View the article online
https://www.science.org/doi/10.1126/sciadv.adh0369
Permissions
https://www.science.org/help/reprints-and-permissions

Use of this article is subject to the Terms of service